THE DETECTION OF FATIGUE DAMAGE ACCUMULATION IN A THICK COMPOSITE BEAM USING ACOUSTO ULTRASONICS

M. Venterink, R. Loendersloot & T. Tinga, *University of Twente, NL*

ABSTRACT

The Acousto Ultrasonics (AU) technique is a Non-Destructive Testing (NDT) technique, widely used for thin, plate-like composite structures. The application of this technique to thick structures, such as the spar cap of rotor blades of wind turbines is considered promising. A problem for the spar caps is fatigue damage. This paper therefore focusses on the fatigue damage detection in a thick composite beam. Two laboratory specimens with a thickness of 56 mm, width of 60 mm and length of 900 mm are equipped with piezo-electric transducers on the top and bottom surface. Short ultrasonic burst waves with varying actuation frequencies are sent by one transducer and measured with the other transducers. Preliminary tests are executed to assess the damage detection capability. The damage is initially simulated by drilling a hole at one location with a stepwise increasing depth of 10 to 56 mm. The number of actuator-sensor paths crossing the simulated damage increases for increasing hole depth. Various Damage Indicator (DI) algorithms and the Reconstruction Algorithm for Probabilistic Inspection of Damage (RAPID) are used for damage assessment and visualisation. A correlation between the DI values and the severity and location of the damage is found. This result is a positive indication for the applicability of AU for damage detection in thick composite structures. A second identical beam is currently placed in a three-point bending fatigue setup.

NOMENCLATURE

Abbreviation	Explanation
AU	Acousto Ultrasonics
CC	Correlation Coefficient
DAQ	Data Acquisition
DI	Damage Indicator
NDT	Non Destructive Testing
NI	National Instruments
RAPID	Reconstruction Algorithm for Probabilistic Inspection of Damage
SAPS	Signal Amplitude Peak Squared
SHM	Structural Health Monitoring
TOF	Time of Flight
WPSD	Welch-based Power spectral Density

1. INTRODUCTION

The rotor blades of a wind turbine are sensitive to damage, especially during operation. This damage can be categorized in accidental and structural damage [1]. Accidental damage can be caused by the environment, e.g. rain droplets causing corrosion on the leading edge of the rotor blade. The structural damage can be caused by the cyclic loading of the system, e.g. fatigue in the spar cap beam of the rotor blades. The latter is a very common defect during operation and is mostly located in the root of the blade. Complex failure mechanisms exist due to the use of composite materials. These failure mechanisms can have large influences on the structural integrity with the problem being that the damage can be invisible from the outside. Increased maintenance efforts have to be taken to assure the structures performance. Structural Health Monitoring (SHM) is a very promising method relying on Non-Destructive Testing (NDT) techniques. The structure can be examined with the use of SHM during operation due to integrated sensors and thus reducing the down time of the wind turbine. The Acousto Ultrasonics (AU) technique is promising to use in SHM. This technique is based on a permanently installed piezo-electric transducer network. Each transducer is sequently used as actuator, while the others act as receiver of the ultrasonic wave(s). Differences in the obtained response signals indicate changes in the structure and can manifest in the time, frequency and modal domain. The differences are caused by damage but could also be caused by for example operational vibrations or environmental temperature changes. The AU technique is already widely used for thin, plate-like structures with promising results [2]. It is also applied on structures with a somehow non-symmetric geometry, i.e. panels or door surroundings with stiffeners [3]. The application of the AU technique to thick structures is however less studied. This work therefore focusses on the fatigue damage detection in a thick composite beam, which

is representative for the spar cap beam of a wind turbine.
Two laboratory scaled specimens are available for experimental testing. The first test object is used for exploratory testing, this will be the focus of this paper. The capabilities of AU for a thick laminate beam are analysed and discussed. Excitation parameters are varied and damage is simulated by drilling a hole with a stepwise increasing depth. This results in a controlled environment with a known damage at only one specific location. AU measurements with the various excitation parameters are carried out for every damage case. The excitations parameters and the sensor locations can be optimized with these results for the second beam. The second object is used to detect fatigue damage before the damage is noticeable by a stiffness degradation derived from force and displacement signals. Therefore the second beam is placed in a three-point bending setup, that is still in operation by the time of writing.
Several Damage Indicator (DI) algorithms are applied between different structure states on all the actuator-sensor paths to assess the damage. These DI values are used for the Reconstruction Algorithm for Probabilistic Inspection of Damage (RAPID) method to visualise the location of the damage in the composite thick beam.

2. EXPERIMENTAL SETUP

An experimental setup has been build that can execute a set of AU-measurements with varying excitation frequencies, see Figure 1.

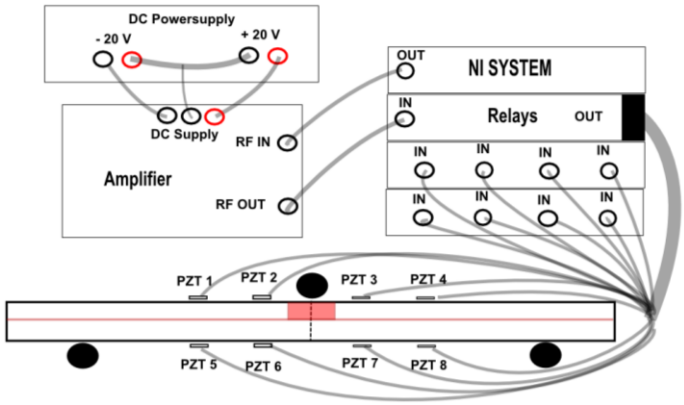

Figure 1: Schematic representation of the measuring setup for beam 2.

The DC power supply is connected to the ADA4870 evaluation board amplifier from Analog Devices. The signal from the function generator is connected to the input of the amplifier. The output of the amplifier is then connected to the relays. The relays has 8 outputs and every output is directly connected with a transducer and an input channel of the NI CompactRio system. The test program controlling the AU measurements can execute one set but is also capable to work fully automated with the system at the knowledge centre Wind turbine Materials and Constructions (WMC), that controls the fatigue test. In this section, the first of the two test specimens is discussed, followed by the data acquisition system from NI with the created LabVIEW software. Finally, the excitation parameters of the AU measurements are discussed.

2.1 TEST OBJECTS

Both beams have the same dimensions: a thickness of 56 mm, a width of 60 mm and a length of 900 mm and are manufactured at WMC. They both contain 96 layers of epoxy resin (Hexion RIM 135) with a UD glass fibre E non-crimp fabric. The locations of the piezo-electric transducers are however different. An example of how the p-876.sp1 transducers of PI ceramic are attached to beam 1 can be seen in Figure 2 [4].

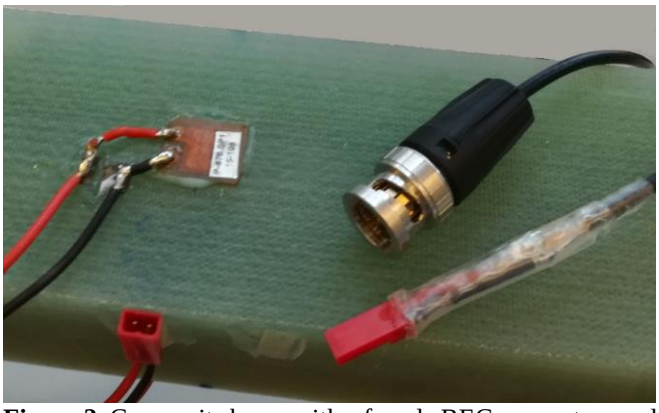

Figure 2: Composite beam with a female BEC connectors and piezoelectric transducers of PI ceramic. The coax cable with the male BEC connector is also shown.

The BEC-connectors are used for practical reasons. Instead of soldering the thin coax cable directly onto the transducers, the BEC male connector is connected to the coax cable. This cable is then attached into the female connecter that is glued on one specific side of each beam.
The first beam has 6 piezo-electric transducers, 5 are bonded to the top surface and 1 is placed on the bottom surface. Damage is first created by drilling a hole with a depth of 10 mm and a diameter of

6 mm, see Figure 3. Since the first beam is used for exploratory testing, the inflicted damage is controlled by drilling a hole. The second beam is placed in the fatigue test for actual real-time monitoring. The results from the first beam are used to optimize:

- The transducer locations.
- The measurement equipment.
- The excitation parameters.

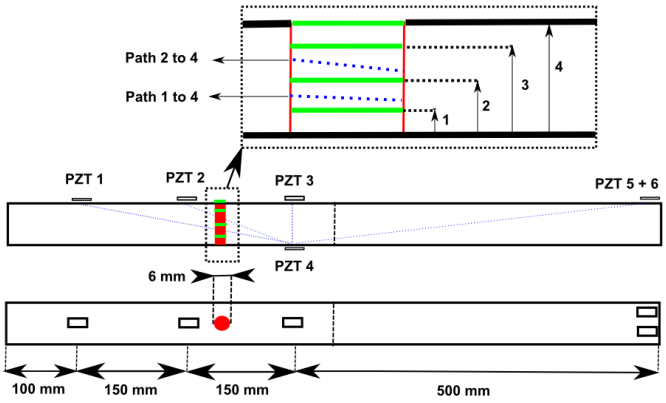

Figure 3: Top: side view of the sensor locations on beam 1 with a detailed view of the hole. The drilled is marked red, with the green lines the different hole depths. The blue lines indicate sensor paths. Bottom: top view.

In the first damage case no actuator-sensor path crosses the hole, see Figure 3. The second damage case has a hole depth of 25 mm and now the path from transducer 1 to 4 crosses the damage. The third damage case has the path from transducer 2 to 4 crossing the damage with a hole depth of 40 mm. Finally in damage case 4 the hole is all the way through the thickness of the first beam. The 5th and 6th transducer are placed on the end of the beam to study the attenuation properties for long(er) propagating distances. The input and output energy can also be more directly compared.

2.2 DATA ACQUISITION SYSTEM

The NI CompactRio data acquisition (DAQ) system controlled by LabVIEW is used. A relays is used to switch the actuation channel over each transducer. For the sampling frequency of 10 MHz the measuring time is limited to 1 ms. A sensor sensitivity of 0.2 V together with a 14 bits resolution results in sufficient accuracy when studying the sensor signals. The maximum output voltage of the NI system is 10 V. The transducers have an operating range from -100 V to 400 V. The output for lower frequencies is sufficient but at increasing actuation frequency it seemed that the NI system cannot provide sufficient power to reach the desired output of 10 V.

2.3 EXCITATION PARAMETERS

The DAQ system is controlled with a custom created LabVIEW software program. The primary excitations parameters can be seen in Table 1. In the following sections only the results of the actuation frequency of 200 kHz are discussed. Primarily the frequency range between 200 kHz and 240 kHz is interesting since it seems that the transducers have an increased impedance here. It is also shown in [2] that excessively strong axial/flexural vibration signals will be generated in the vicinity of their respective natural frequency range with impedance measurements. This will increase the damage detection capabilities.

Table 1: Excitation parameters for the AU measurements on beam 1.

Parameter	Value
Frequency	40 kHz - 340 kHz Δ20 kHz
Amplitude	10 V
Cycle Numbers	3.5
Averages	10
Measurement time	1 ms
Pre-sampling	0.1 ms

3. SIGNALS

The sensor signals which are retrieved when using the actuation parameters in Table 1, are discussed in this section. First the pristine signals from the reference state, followed by the most interesting deviations in sensor signals caused by the different damage states. The exact nature of the waves will not be studied. It is well known that lamb waves propagate in thin plate like structures, but the ultrasonic waves in a thick (steel) structure are more complex [5, 6]. The usage of composite materials in the present work will further increase the complexity.

3.1 PROCESSING

Before the sensor signals can be analysed, they have to be processed. The noise is reduced by applying averaging. Unwanted frequencies below 5 kHz and above 500 kHz are filtered out with a 12th order Butterworth filter, see Figure 4. This

filter is applied two times to prevent a phase delay. It is chosen due to the constant gain in the passband and no ripple around the cut-off frequency. The offset is removed by subtracting the mean of the entire signal from every value. The crosstalk around 0.1 ms caused by the relays can be seen in Figure 4 and will not be filtered out.

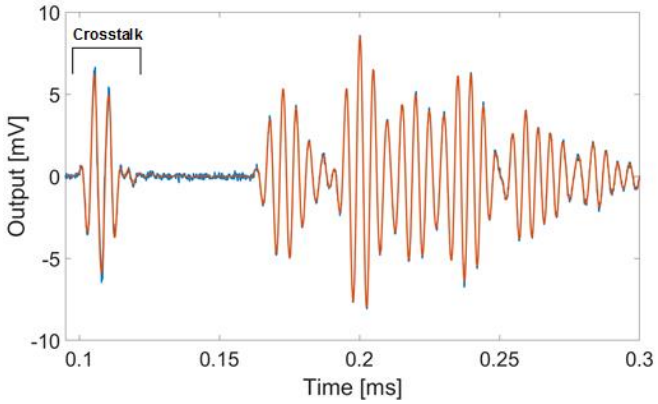

Figure 4: An example of a sensor signal before (blue) and after (red) filtering with a 12th order Butterworth filter.

3.2 RESULTS

The pristine response signals can be seen in Figure 5 using transducer 1 as actuator. The first wave package at sensor 2 is in amplitude the greatest of all wave packages in that signal. The magnitude of the first wave package relative to the second wave package in its signal, reduces with increasing propagating distance. This is also concluded in [5] and [7], though the used material there is steel.
The transducers 3 and 4 are located symmetrically on the top and bottom surface. The Time of Flight (TOF) of the wave packages would be equal in the case of lamb waves in a thin plate-like structure. Apparently, at 200 kHz the waves are not pure lamb waves in the thick composite beam.

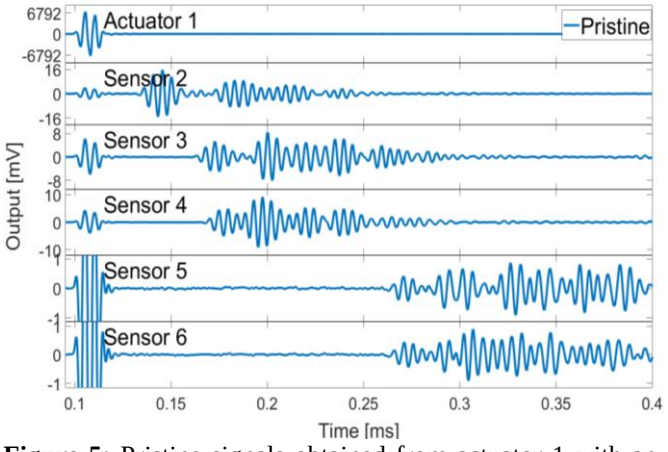

Figure 5: Pristine signals obtained from actuator 1 with an actuation frequency of 200 kHz.

Using transducer 4 as actuator also gives some interesting results, see Figure 6. All sensors are now situated on the other side of the beam. For increasing propagation distances, a relative increase of the first wave package amplitude is observed. This is exactly the contrary as found in [5]. A possible explanation is that shear waves (the second wave package) propagate more easily through the thickness at these short distances.
The signals from sensor 5 and 6 are expected to be exactly the same. This indicates that the exact location (on the width of the beam) and the gluing process already have an influence on the sensor response. Furthermore, sensor 5 and 6 show a relative low amplitude on long propagating distances. They will therefore not be included in this paper. Most probably the high attenuation of the waves in a composite material restricts the maximum distance between transducers.

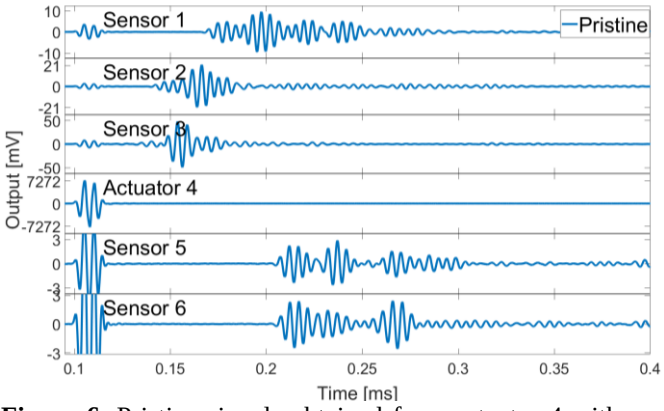

Figure 6: Pristine signals obtained from actuator 4 with an actuation frequency of 200 kHz.

The biggest difference in the signals due to the damage can be found on path 1-4 at around 0.2 ms, see Figure 7. Interesting to see is how this deviation increases with increasing hole depth, see Figure 3. The magnitude of the first wave package of damage case 1 and 2 is related and almost similar.

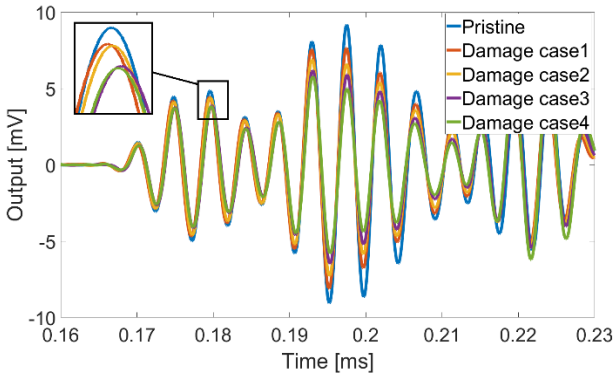

Figure 7: The pristine reference signal with the 4 damage cases of sensor 4 and actuation 1 at 200 kHz.

The first wave package is clearly equally affected by the damage located directly on or next to the direct transducer path 1 to 4. Increasing the damage to damage case 3 and 4, results in another equal reduction of the magnitude of the first wave package. Apparently the first wave package has a specific area in the beam by which it can be influenced by the damage.

The signal on sensor 3 with 1 as actuator for all damaged states can be seen in Figure 8. The deviations around 0.2 ms are once more related to all the hole depths, see Figure 3. Especially interesting is again the decrease of the first wave package on this surface path 1-3. The first wave is hardly affected until the drilled hole reaches the surface. Again it shows that the first wave package is only influenced by a specific area of the beam.

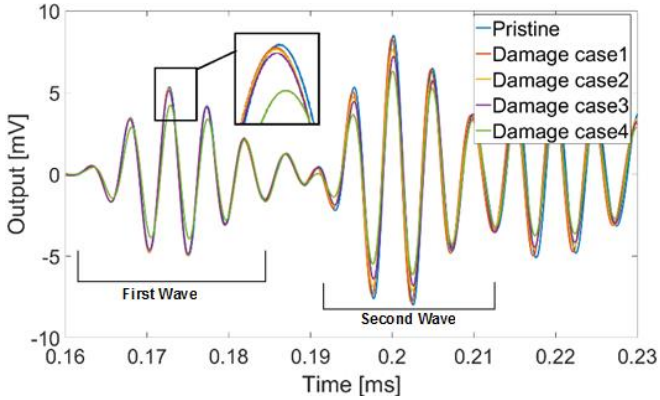

Figure 8: Response signals on sensor 3 of beam 1. Actuation channel is 1 with a frequency of 200 kHz.

A decreasing amplitude with a phase change behind the first wave package on sensor path 1-2 from damage state 3 to 4 is observed, see Figure 9. This could relate to a reflection when the hole reaches the surface since the damage is not present on its direct path. At 0.2 ms the magnitude of the response increases for increasing damage state which could also be a reflection of the damage [2].

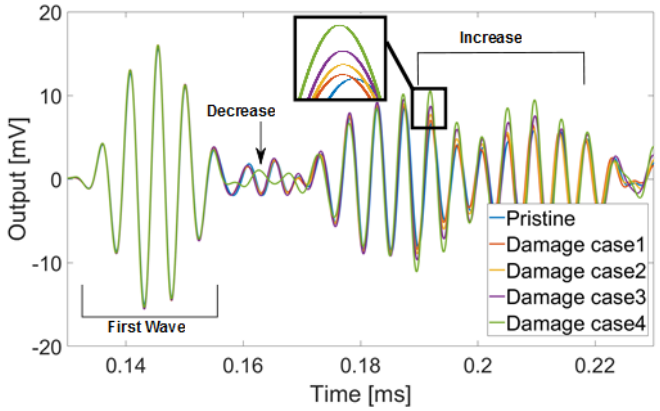

Figure 9: The pristine reference signal with the 4 damage cases of sensor 2 and actuation 1 at 200 kHz.

From this section it can be concluded that the AU-measurements are sensitive to damage accumulation created by drilling a hole.

4. DAMAGE INDICATORS

The deviations in the response signals due to damage are clearly visible in the figures from the previous section. The next step is to analyse and process these changes to detect and quantify the damage. This is done by relating a current damaged state with the pristine state of the structure. The comparison between the two signals is translated into a Damage Indicator (DI). Ideally, this DI has the value of 1 when there is no (extra) damage compared to the referenced pristine structure and has a decreasing DI when there is damage present. This DI is a value on a specific actuator and sensor path between two structure states. Different DI algorithms are already used in the literature [8]. All of those mentioned in [8] are also used in this project but only the most interesting ones are discussed for an actuation frequency of 200 kHz. Small changes are applied to the DI in this work due to problems also discussed in [8].

4.1 CORRELATION COEFFICIENT

The Correlation Coefficient (CC) algorithm is already successfully applied to a plate-like structure [8]. This method is implemented on three different ways in this work, see Table 2.

Table 2: Different implementations of the CC algorithm [8] **between channel *i* and actuation channel *j*.**

CC	Expression
$DI_1(i,j)$	The entire time interval.
$DI_2(i,j)$	Time interval is located 0.1 ms around the maximum wave package.
$DI_3(i,j)$	Similar to DI_2 and scaled with C.

The DI_3 algorithm (CC3) is similar to the DI_2 (CC2) but it has a scaling factor C for the longer propagating distances such that it reduces the DI value. This factor is equal to:

$$C = \frac{\mu_k}{A_k} * \frac{A_i}{\mu_i}, \quad (1)$$

with A_i the maximum amplitude of sensor i and μ_i the noise level of sensor i. The sensor with the highest maximum amplitude of a single AU

measurement is noted as k. This factor thus makes sure that the strongest signal is multiplied with '1'. Assuming that the noise level of every channel is equal, the factor reduces to:

$$C = \frac{A_i}{A_k} \tag{2}$$

The results on the first beam are however not so promising as compared to [8], see Figure 10. Transducer 1 is used as actuator and it is expected due the damage location that sensor 3 and 4 give lowered DI values and sensor 2, 5 and 6 give DI values of 1. This is however not the result obtained with CC2 and it suggests that there is no relation with the location of the damage. The CC3 shows however to be more promising than CC2 when comparing Figure 10 (a) and (b).

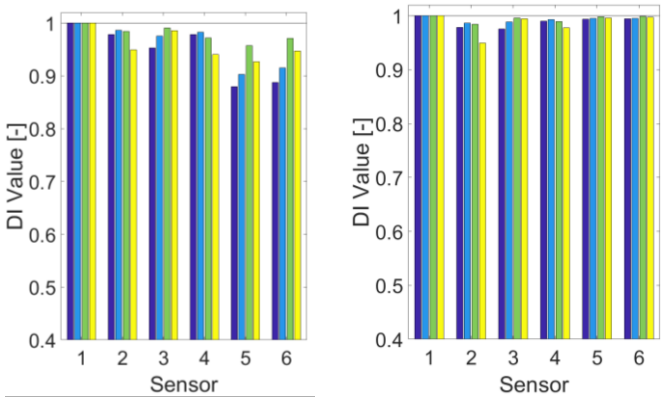

(a) CC2. **(b)** CC3.

Figure 10: DI results at 200 kHz with transducer 1 as actuator. The four colours represent the 4 damage cases. Blue is damage case 1 and yellow is damage case 4.

Furthermore the DI value does not decrease with increasing damage case. The latter suggest that the CC DI has no relation with the severity of the damage. This could be explained by looking more closely at the time signals. A (small) phase delay is present between different measurements and this likely causes large deviations in the DI. The next section will show that the DI algorithms based on amplitude are much more sensitive.

4.2 SAPS

The Signal Amplitude Peak Squared Percentage Differences (SAPS) algorithm as used in [8] is also implemented. This SAPS is changed for the current structure to improve its performance. Due to the deviations in the damaged sensor responses, the maximum of the entire signal can happen for every damaged state on different times. This maximum can also have slight phase delay. This phase delay can have different causes. Therefore DI_2 algorithm (SAPS2) focuses on the maximum of the healthy signal and compares it with the maximum of the damage state around the same time:

$$DI_2(i,j) = 1 - \left(\frac{\max[S_{H,i}] - \max[S^{\tau}_{D,i}]}{\max[S_{H,i}]}\right)^2, \tag{3}$$

with:

$$S^{\tau}_{D,i} = S_{D,i}\left(t^{H,i}_{max} - \Delta t_{small} : t^{H,i}_{max} + \Delta t_{small}\right), \tag{4}$$

and with $S_{H,i}$ is the healthy signal from sensor i, $t^{H,i}_{max}$ is the time of the maximum value of the healthy signal from sensor i, the damaged state is denoted by D, j indicates the actuation sensor and Δt_{small} is equal to the length of 2 oscillations cycles of the actuation frequency. SAPS2 searches for the maximum in the damaged state near the maximum of the reference data with an offset.

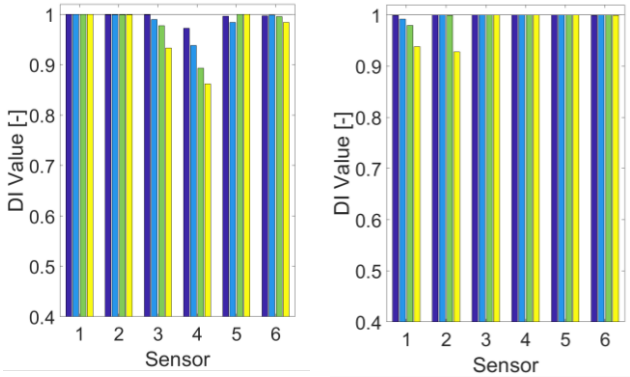

(a) Actuation by sensor 1. **(b)** Actuation by sensor 3.

Figure 11: DI from beam 1 SAPS2 200 kHz. The four colours represent the 4 damage cases. Blue is damage case 1 and yellow is damage case 4.

It is expected that damage is not identified on a surface transducer path 1-3 for damage case 1 to 3. However it seems that damage under the surface can also be identified on that sensor path for damage case 2 and 3, see Figure 11. On the surface path 3-2 only surface damage can be detected, see Figure 11 (b). This indicates that damage under the surface is not detected by short propagating distances. The waves have more penetration for increasing propagating distances.

On damage path 1-4 all damage cases can be detected, which was also expected. The amount of damage is related to the magnitude of the DI for a through-the-thickness path. This is not the case for

the CC for the current application, as can be seen in Figure 10. SAPS2 is an big improvement even though it still shows small irregularities in the DI for large propagating distances. The DI on sensor path 1-5 and 1-6 seem to be insensitive to (the magnitude of) the damage, see Figure 11 (a). This likely caused by the relatively high amount of noise.

4.3 WPSD

Interesting to note is that DI algorithms based on the frequency content also give promising results. The Welch-based Power spectral Density (WPSD) algorithm is an example and is also used in [8]. Using the entire signal (WPSD1) does not give the best results, see Figure 12(a). Sensor 2 has decreased DI values that are not expected. Focussing on a specific interval increases its performance, see Figure 12(b). WPSD2 focusses on the interval starting after the crosstalk until the wave package that is 20 times smaller than the maximum wave package. The frequency resolution is low when considering the sampling frequency of 10 MHz and only 4000 data points. Even though the shorter propagating distances do seem to have a relation between the amount of damage and the WPSD2 values (sensor 3 and 4).

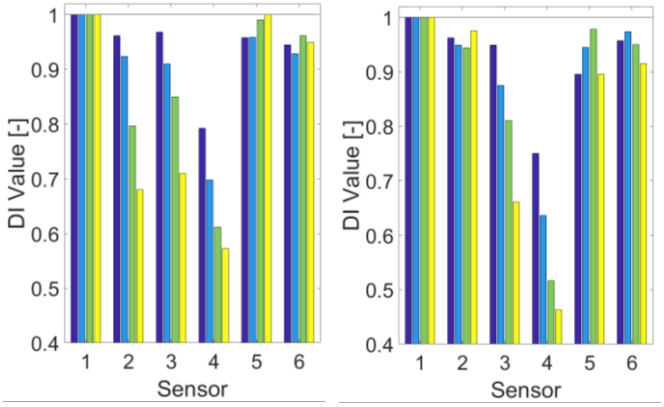

(a) WPSD1. **(b)** WPSD2.

Figure 12: DI from beam 1 WPSD2 200 kHz. The four colours represent the 4 damage cases. Blue is damage case 1 and yellow is damage case 4.

Comparing the results from WPSD2 (Figure 12(b)) and SAPS2 (Figure 11(a)), it shows that they give very similar results. However, WPSD2 has decreased DI's on all the four damage cases on sensor path 1-2 where SAPS2 produces the expected DI values of 1. Finally it can be concluded that the SAPS2 is the most sensitive to the location and severity of the damage for the current structure. WPSD2 shows to be promising but still gives unexpected result on the non-damaged paths. The reliability has to be investigated to fully understand the results due to the mentioned low frequency resolution. Therefore SAPS2 will be used in the RAPID algorithm in the next section.

5. RAPID

In this section the results from SAPS2 are implemented in the modified RAPID method as used in [8] and [9]. First the RAPID method is explained, followed by the results.

5.1 METHOD

A grid is defined that overlays the side of the beam. The damage intensity $I(x,y)$ at each grid point (x,y) is calculated. Every actuator-sensor path has a specific area of influence. The damage intensity is defined as in [9]:

$$I(x,y) = \sum_{k=1}^{N_p}(1-DI_k)\left(\frac{\beta - R(x,y)}{\beta - 1}\right), \qquad (5)$$

with DI_k being the DI of the k^{th} actuator-sensor path, N_p the number of paths and a scaling factor β determining the area of influence. The elliptical distribution function $R(x,y)$ is used as in [9]:

$$R(x,y) = \frac{\sum_{k=i,j}\sqrt{X+Y}}{(1-2\alpha)\sqrt{\Delta x_{nm}^2 + \Delta y_{nm}^2}}, \qquad (6)$$

$$X = (\Delta x_k + q\alpha\Delta x_{nm})^2, \qquad (7)$$

$$Y = (\Delta y_k + q\alpha\Delta y_{nm})^2, \qquad (8)$$

$$\Delta x_k = x - x_k, \qquad \Delta x_{nm} = x_n - x_m, \qquad (9)$$

with $k = n, m$ and (x_n, y_n) and (x_m, y_m) the locations of transducers n and m. If $R(x,y) < \beta$, $q = 1$ for $k = i$ and $q = -1$ for $k = j$ and $R(x,y)$ equals β if $R(x,y) \geq \beta$. The scaling factor α compensates too high damage indications near the location of the transducers. For the current work α and β are chosen to be equal to β=1.16 and α=0.25. These values do give good results but still have to be optimized as in [9]. All the actuator-sensor paths are used, with Figure 11 (a) being an example from actuator 1 to sensor 2 to 6.

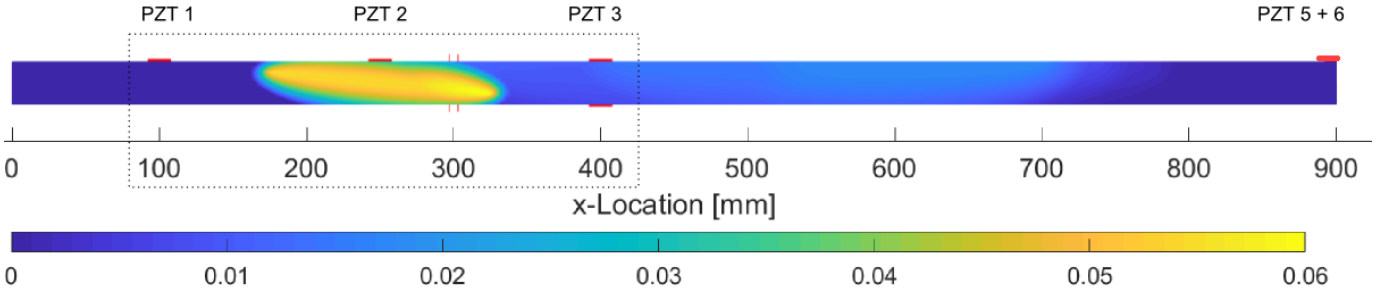

Figure 13: The damage intensity $I(x, y)$ for damage case 1 using SAPS2 at 200 kHz. The colour bar shows which colours belong to which intensity. The red dots are the 6 piezo-electric transducers. The location of the drilled hole is highlighted with red lines.

5.2 RESULTS

The RAPID plot for damage case 1 using SAPS2 can be seen in Figure 13. In the regions with the blue colour no damage is predicted, and the yellow area is the location with the highest probability of damage. The predicted damage location is large and not very accurate. This can be explained by looking at the transducer and damage locations. Since there is only 1 transducer on the bottom surface, there is also less 'information' on this damaged side of the beam. The RAPID method therefore fails to predict the exact hole dimensions that can be seen in Figure 3.

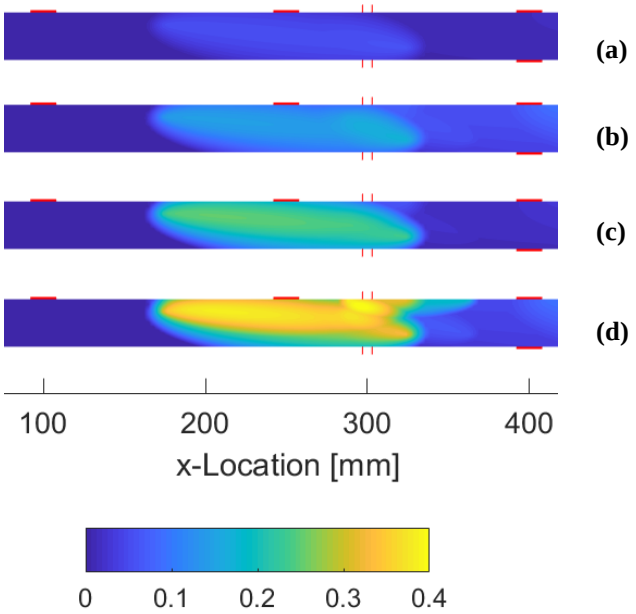

Figure 14: RAPID plot for damage case 1 (a), 2 (b), 3 (c) and 4 (d) using SAPS2 at 200 kHz.

The highlighted area from Figure 13 is used in Figure 14. Damage case 1 can again be seen together with the other 3 damage cases on an equal scale. The damage intensity $I(x, y)$ increases for increasing damage case. The location is however not predicted properly in any damage case due to previous mentioned lack of sensors and the inaccuracy of sensor 5 and 6 over the long propagating distances. The fact that there is also a high probability of damage predicted between sensor 1 and 2 can be explained by looking at Figure 11 (b), the DI's are lower at sensor 1 than at sensor 2. The latter is also discussed in section 4.2. Comparing Figure 14 (c) and (d) shows however that the 'extra' surface damage going from damage case 3 to 4 is predicted quite accurate.

6. FATGIUE TEST

The second beam will be placed in the 3-point bending setup at WMC. The sensor placement on the second beam is optimized based on the results from section 3, 4 and 5. The maximum propagating distance is 350 mm and there are 4 transducers placed on the top and bottom, see Figure 15. The DI and RAPID algorithms can give a more accurate representation of the damage location through the thickness. Only eight transducers are used since this is the maximum currently supported by the DAQ system. During the measurements on beam 1, the DAQ shows to have a power restriction at higher frequencies as previously stated in section 2.2. The desired parameters of 10 V and 3.5 oscillations used for the function generator are not fulfilled by the actuation transducer at 200 kHz.

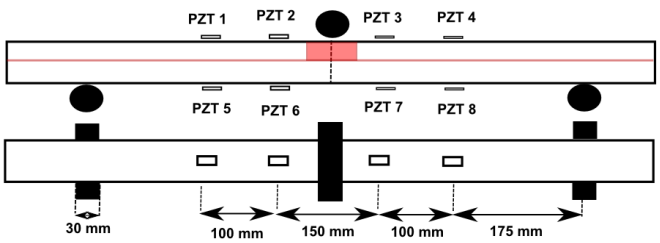

Figure 15: Side and top view of the second beam with the sensor locations. The red area highlights the possible damage locations.

To overcome this power restriction problem, the ADA4870 evaluation board from Analog Devices is used. The actuation signal of 200 kHz can be seen in Figure 16 with and without using the amplifier.

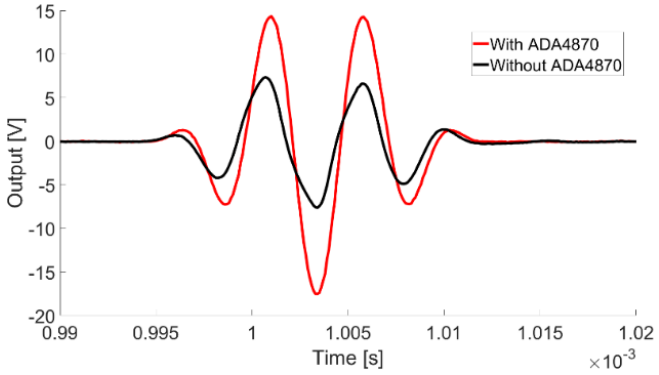

Figure 16: Actuation signals of 200 kHz without amplifier (black) and with the ADA4870 amplifier (red).

This amplifier is capable of enhancing the maximum output from 10 V to approximately 18 V with a sufficiently high slew rate. The maximum amplified output is still frequency depended but the variance decreases a lot. Without the amplifier the actuation voltage ranges between 5.39 V for 340 kHz to 10 V at 20 kHz. With the amplifier this is 16.8 V to 18.1 V. Note that the NI system can only measure up to 10 V, therefore a Handyscope HS3 is used to obtain the results in Figure 16.

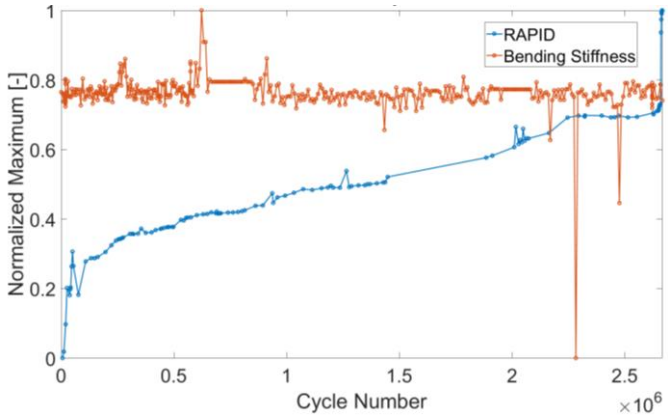

Figure 17:The normalized maximum of the RAPID plot using 200 kHz and SAPS2 is plot against the cycle number of the fatigue test. The same is done for the normalized maximum of the bending stiffness.

Currently the fatigue test is running at WMC with the second beam and the first results are still being analysed. The first analysis does show however that the AU measurements are executed successfully. The responses obtained show at least to be sensitive to the damage accumulation for increasing cycle number of the fatigue test. The deviations in the response signals are however more diverse than on beam 1. The maximum value of the RAPID plot of each measurement using 200 kHz is plotted in Figure 17. The bending stiffness extracted from the force and displacement signals is also shown. The AU measurements show an increase, while the stiffness remains constant. This indicates that AU can be used for early detection of accumulating damage.

7. CONCLUSIONS & FUTURE PROSPECTS

The damage detection capabilities of the AU-measurements have proven to be successful on a thick composite beam with a drilled hole.

- The amplitude and frequency content is sensitive to the severity of the damage.
- The first wave package contains information on the location of the damage.
- The magnitude of the second wave package is related to the severity of the damage.
- The modified SAPS2 DI is more sensitive to the severity and location of the damage than CC and WPSD.
- A symmetric distribution of transducers is best. This is applied on beam 2.
- The RAPID plot for 200 kHz gives an inaccurate representation of the damage but is sensitive to damage accumulation.

Currently, the second beam with an optimized sensor placement is placed in the fatigue machine at WMC and AU-measurements are executed. The measurements show to be sensitive to the accumulation of fatigue induced damage. The response signals have to be analysed more carefully before final conclusions can be drawn since the changes in the signals due to the damage are more complex than on beam 1. In future work, the algorithms have to be improved for increased damage localisation and detection capabilities using amplitude and frequency content of the response signals.

ACKNOWLEDGEMENTS

The work presented is funded by the Dutch TKI Wind at Sea project SLOWIND, grant number TEWZ 115012. This support is gratefully acknowledged by the authors. The authors in addition acknowledge the knowledge centre WMC for providing the test articles.

REFERENCES

[1] F. Lahuearta, “Identification of typical failures in composite rotor blades and structural health monitoring,” Technical Report project SLOWIND, Knowledge center WMC, Wieringerwerf, The Netherlands, 2016.

[2] X. L. Liu, Z. W. Jiang and L. Ji, “Investigation on the Design of Piezoelectric Actuator/Sensor for Damage Detection in Beam with Lamb Waves,” *Experimental Mechanics*, vol. 53, no. 3, pp. 485-492, 2013.

[3] M. Moix-Bonet, B. Eckstein and P. Wierach, “Probability-Based Damage Assessment on a Composite Door Surrounding Structure,” in *8th European Workshop On Structural Health Monitoring (EWSHM)*, Bilbao, Spain, 2016.

[4] PI Ceramic GmbH, *Technical Note DuraAct Patch Transducers P876*, Lederhose, Germany, 2017.

[5] D. W. Greve, I. J. Oppenheim and P. Zheng, “Lamb Waves and Nearly-Longitudinal Waves in Thick Plates,” in *Proceedings of SPIE - The International Society for Optical Engineering*, United States, 2008.

[6] V. Giurgiutiu, Structural Health Monitoring with Piezoelectric Waver Active Sensors, Columbia, SC, USA: Elsevier, 2008, pp. 622-623.

[7] Y. Ying, I. J. Oppenheim, J. H. Garrett, D. W. Greve and L. Soibelman, “Oblique excitation of nearly-longitudinal waves in thick plates,” in *SPIE Smart Structures and Materials*, San Diego, California, United States, 2010.

[8] R. Loendersloot and M. Moix-Bonet, “Damage identification in composite panels using guided waves.,” in *Challenges in European Aerospace*, Delft, The Netherlands, 2015.

[9] M. Moix-Bonet, B. Eckstein, R. Loendersloot and P. Wierach, “Identification of barely visible impact damages on a stiffened composite panel with a probability-based approach.,” in *The International Workshop on Structural Health Monitoring*, Stanford, USA, 2015.